Influence of Non-newtonian Properties of Liquid in Microchannels on Pressure Drop and Bubble Length

Gang Yang
DMU: Dalian Maritime University https://orcid.org/0000-0003-2383-7375
Kai Feng
DMU: Dalian Maritime University
Jia-Pei Li
DMU: Dalian Maritime University
Yu-Hang Gao
DMU: Dalian Maritime University
Hui-Chen Zhang (hczhang@dlmu.edu.cn)
Naval Architecture and Ocean Engineering College, Dalian Maritime University

Original Article

Keywords: Microchannel, Non-Newtonian fluid, Gas-liquid two-phase flow, Pressure drop, Bubble length

Posted Date: October 28th, 2021

DOI: https://doi.org/10.21203/rs.3.rs-1015177/v1

Title page

Influence of non-Newtonian properties of liquid in microchannels on pressure drop and bubble length

Gang Yang, born in 1996, is currently a Ph.D. candidate at *Naval Architecture and Ocean Engineering College, Dalian Maritime University, China*. He received his bachelor's degree from *Fuzhou University, China*, in 2018. His research interests focus on microfluidic devices.
E-mail: 1186593481@qq.com
Tel: +86-18641125619

Kai Feng, born in 1988, is currently a Ph.D. candidate at *Naval Architecture and Ocean Engineering College, Dalian Maritime University, China.*
E-mail: fengkai@dlmu.edu.cn

Jia-Pei Li, born in 1994, is currently a master candidate at *Naval Architecture and Ocean Engineering College, Dalian Maritime University, China.*
E-mail: 504961331@qq.com

Yu-Hang Gao, born in 1996, is currently a master candidate at *Naval Architecture and Ocean Engineering College, Dalian Maritime University, China.*
E-mail: 3222511387@qq.com

Hui-Chen Zhang, born in 1965, is currently a professor and a Ph.D. candidate supervisor at *Naval Architecture and Ocean Engineering College, Dalian Maritime University, China.* He received his bachelor's degree and master's degree from *Shenyang Polytechnic University, China*, in 1987 and 1990, respectively. He received his Ph.D. degree in mechanical design and theory from *Xi'an Jiaotong University, China*, in 1993. His research interests focus on microfluidic devices and nanotribology.
E-mail: hczhang@dlmu.edu.cn
Tel: +86-15542672593

Corresponding author：Hui-Chen Zhang　E-mail：hczhang@dlmu.edu.cn

ORIGINAL ARTICLE

Influence of non-Newtonian properties of liquid in microchannels on pressure drop and bubble length

Gang Yang • Kai Feng • Jia-Pei Li • Yu-Hang Gao • Hui-Chen Zhang

Received June xx, 202x; revised February xx, 202x; accepted March xx, 202x

Abstract: Pressure drop and bubble morphology are essential characteristics of microfluidic system design and process control. In this paper, a new type of microfluidic chip was designed and produced, including a flow-focusing device and a fluid transport device to simulate bubble generation and fluid transport in practical applications. Nitrogen and sodium carboxymethyl cellulose solutions of different concentrations were used as the gas and liquid phases. Single-phase flow and two-phase flow experiments were designed according to the commonly used flow conditions in the microchannel. By changing the flow rates of liquid and gas, the pressure drop in the fluid transport device of the two fluid states, the length of the bubble generated in the flow-focusing device, and the length of the bubble after passing through the transport device were measured, respectively. The influence of non-Newtonian characteristics of the liquid on pressure drop and the length of the generated bubbles were analyzed. The results show that the non-Newtonian characteristics of fluid have a significant effect on the pressure drop of single-phase flow and two-phase flow. Within a specific flow velocity range, the bubble length can be predicted according to the dimensionless number of the liquid. The pressure drop increases the bubble length to varying degrees.

Keywords: Microchannel • Non-Newtonian fluid • Gas-liquid two-phase flow • Pressure drop • Bubble length

1 Introduction

Microfluidic technology has broad application prospects and potentials in the fields of biomedicine, environmental monitoring and microelectronics [1][2][3]. In the microfluidic system, the microchannel is an indispensable component, which can reduce the difficulty of control transfer and improve the efficiency and safety of the production process [4][5]. Two-phase flow is often involved in micro-reactors, micro-electromechanical systems (MEMS), electronic circuits and cooling systems of micro-fuel cells. In the past, numerical and experimental studies on gas-liquid two-phase flow in microchannels were mainly gas-Newtonian phases [6][7]. However, non-Newtonian fluid is involved in almost all industrial and biological applications, such as polymer solutions, blood and wastewater. Due to the size effect of the microchannel, the Reynolds number of the internal fluid is small, the shear rate is high, and the rheological properties of the non-Newtonian fluid have a more significant influence on the flow behavior of the liquid in the microchannel. These make the study of the gas-non-Newtonian fluid in the microchannel more attractive [8].

The gas-non-Newtonian fluid two-phase flow research mainly focuses on the pressure drop in the microchannel and the flow pattern (the shape of bubbles or droplets).

The overlooked phenomena in the macro-scale fluid analysis have a significant impact on the movement of the fluid in the microchannel, such as pressure drop, liquid surface tension, and non-Newtonian properties. The microchannels' structural design and operation requirements need to consider the influence of pressure drop [9]. Guo et al. [10] proposed a new two-phase pressure drop model in a tree-shaped mass transfer microchannel to predict fluid dynamics in a tree-shaped microchannel under gas-liquid two-phase flow. Mondal et al. [11] studied the pressure drop characteristics of single-phase flow and water-organic liquid

✉ Hui-Chen Zhang
hczhang@dlmu.edu.cn
[1]Dalian Maritime University, Dalian 116026, China

two-phase flow through rectangular snake-shaped microchannels and established an empirical model. The operating variables were used to predict the single-component and multi-component fluid's pressure drop and friction coefficient. James et al. [12] studied the pressure drop characteristics of the air-water two-phase flow in a linear microchannel and compared the two-fluid model with the pressure drop value of the two-phase flow. They proved that the two-fluid model could predict the pressure drop of two-phase flow in the microchannel, and the error is less than 3.25%. Li et al. [13] analyzed the correlation between the pressure drop prediction model and the operating variables, taking the two-phase flow Reynolds number, viscosity and gas content as the variables of the prediction model, which proved the accuracy of the prediction model. Agus et al. [14] studied the flow characteristics of non-Newtonian fluid two-phase flow in a horizontal rectangular microchannel with a sudden expansion structure. They used a pressure sensor to measure the pressure distribution before and after the sudden expansion. The pressure drop caused by the expansion was discussed.

Precise control and manipulation of the volume of bubbles (droplets) in the microchannel are vital for the application of microfluidic technology [15][16][17]. Behnam et al. [18] experimentally studied the generation of Newtonian and non-Newtonian droplets flowing through the micro-intersection in the continuous silicone oil phase. They discussed the influence of the viscosity and shear-thinning characteristics of the non-Newtonian fluid dispersed phase on the droplet state. It is shown that the droplet volume is related to the capillary number of the continuous phase and the flow rate ratio of the two phases. Through experiments, Cao et al. [19] analyzed the flow state of a liquid-liquid two-phase flow in a cross microchannel. Through force analysis, the mechanism of flow pattern formation was explained. On this basis, the dimensionless analysis of Weber number and Reynolds number were carried out, and the flow pattern conversion criterion was obtained. At the same time, the influence of velocity ratio, Weber number, Reynolds number, and hydraulic diameter on droplet volume was also analyzed. Somasekhara et al. [20] proposed a three-dimensional model based on fluid volume to study the formation of droplets in microfluidic T-shaped structures. Various factors affecting the formation of droplets were analyzed, such as continuous phase and dispersed phase flow, interfacial tension and non-Newtonian rheological parameters. The research found that rheological parameters had an important influence on droplets' length, volume, and formation process. With the increase of the effective viscosity, the frequency of droplet formation increases, and the length of the droplet decreases with the rise of the continuous phase flow. With the increase of surface tension, the droplet size increases.

In summary, although considerable research has been conducted on the pressure drop and flow pattern in the microchannel, the regulation of pressure drop and flow pattern and the relationship between the two still need to be deepened. This paper designed a new type of microfluidic chip, including flow focusing and fluid transport, to simulate bubble generation and fluid transport in practical applications, focusing on the pressure drop in the channel and bubble generation length and the change of bubble length.

This research analyzed the influencing mechanism of the non-Newtonian characteristics and the working conditions on the pressure drop and bubble length in the microchannel. Clarify the influence of the pressure drop on the bubble length during the bubble transfer process.

2 Experiments

The microfluidic chip configuration structure is shown in Figure 1. The microchannel includes a cross-shaped bubble generating part and a snake-shaped bubble transport part. The width and depth of the microchannel are 0.3mm, and the unit of dimensions in the figure is mm. The material of the chip is polydimethylsiloxane (PDMS), which is prepared by photolithography technology. The main processing flow path is Photoresist pre-baking - Covering mask exposure -Developing template -PDMS covering-Chip peeling - Organic glass (PMMA) packaging. The surface roughness of the microchannel after processing is $Ra \leqslant 0.2\mu m$.

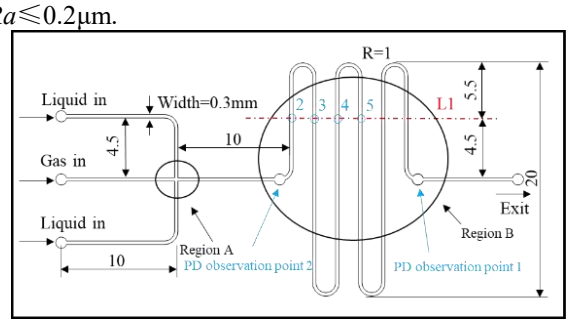

Figure 1 Configurations of the microfluidic chip

In the experiment, sodium carboxymethylcellulose (CMC) solutions with mass fractions of 0.1%, 0.2% and 0.3% were prepared as the non-Newtonian liquid, distilled water was used as the Newtonian liquid phase, and the gas phase was nitrogen. A pipette and an electronic balance were used to measure the density of the liquid. A surface tension meter (K100C, KRUSS, Germany) was used to measure the surface tension of the liquid. A rheometer (MCR301, Anton

Paar, Austria) was used to measure the viscosity change of CMC solution under different shear rates. The Ostwald-de Wale power-law model was used to fit the power-law equations of three non-Newtonian fluids to determine their consistency coefficients and flow characteristics index.

$$\mu = k\left(\gamma\right)^{n-1} \tag{1}$$

where γ represents the shear rate(1/s), μ represents the dynamic viscosity(N·s/m^2), k is the consistency coefficient, and n is the flow characteristic index.

The experimental system is shown in Figure 2. The liquid was input to the chip using an advection pump (2PB, XingDa Technology, Beijing). After the pressure of gas was reduced by a pressure reducing valve, a gas flow meter (MQV9005, Azbil, Japan) was used for the control of the flow rate. Two pressure drop monitoring points were set in the experiment, as shown in Figure 1 (PD observation point1 and PD observation point2). The pressure drop between the two points was measured using a pressure sensor (PX409-0150WUV, Omega, America) to obtain the pressure drop of the serpentine shape part of the microchannel. Two observation points of bubble length were set, respectively located in the cross bubble generating part (Region A) and the serpentine part (Region B). A high-speed camera (HotShot 512sc, DAC, America) was used for observation and analysis. The data acquisition system adopts a low-voltage DC power supply, using an L7824 voltage-stabilizing transistor for voltage stabilization.

The experimental steps were as follows: (1) Use hoses, steel needles, sealants, wires, etc., to connect the microchannel system according to the testing device diagram, check the airtightness of the device and check the on-off of the test circuit. (2) Fix the microchannel chip on the fixture, use a high-speed camera to aim at the shooting area and adjust the focus. Adjust the pressure compensation value of the pressure sensor on the data collector. (3) Turn on the cold light source, high-speed camera and image acquisition software in turn, and set the shooting frame rate to 3×10^4fps; (4) The liquid-phase speed range: 0.25 ml/min~2 ml/min (the single-phase flow experiment is 0.25 ml~4 ml/min), gas-phase speed range: 0.25 ml/min~4 ml/min.

In order to analyze the changes of the flow field in the microchannel and the dynamic characteristics of the bubble more deeply, a numerical simulation of the movement process of the N_2-CMC solution two-phase flow in the microchannel was carried out. A 1:1 two-dimensional model was constructed according to the size of the microchannel chip, and the gas and liquid inlet speeds were set to be 1 ml/min. When setting the liquid viscosity, non-Newtonian-power-law viscosity model and the viscosity calculation parameter corresponding to 0.3%CMC solution were used. Because the Reynolds number of the fluid in the microchannel is small, the laminar flow model was chosen, and the VOF model was chosen to solve the NS and the continuous phase equations. The PISO algorithm was selected for the pressure-velocity coupling equation. The PRESTO algorithm was chosen for the pressure discrete equation. The first-order upwind style was chosen for the momentum equation, and the time step was set to 1×10^{-7}s.

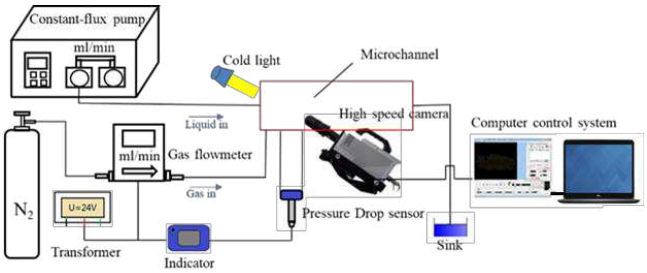

Figure 2 Experimental system

Nomenclature

γ	shear rate
μ	dynamic viscosity
k	consistency coefficient
n	flow characteristic index
Re^*_L	dynamic Reynolds number
We	dynamic Weber number
Ca^*_L	dynamic capillary number
ρ_L	liquid density
d	hydraulic diameter
v_L	liquid velocity
a	constant
b	constant
P_d	pressure drop gradient
P_D	pressure drop between the two pressure monitoring points
P_{sd}	pressure drop gradient of single-phase flow
P_{td}	pressure drop gradient of two-phase flow
S	distance the two pressure monitoring points
Q_L	liquid flow rate
Q_G	gas flow rate
μ_G	gas viscosity
v_G	gas velocity
W_d	width of the bubble neck
L	bubble length
P_D*	pressure drop between 2 and 5
S*	distance between 2 and 5

3 Results and discussion

The measured physical properties of the liquid phase are shown in Table 1. The densities of the four liquids are relatively similar, so the difference in inertial force effects is slight. The surface tension of CMC solution is less than water, but the consistency coefficient is larger than water and the higher the concentration, the greater the consistency

coefficient. The flow characteristic index of the three CMC solutions is less than 1, which belongs to the shear-thinning fluid category in the non-Newtonian fluid.

Table 1 Characteristic parameters of liquid phase

Liquid phase	Density, ρ (kg/m^3)	Surface tension, σ (mN/m)	Fluid consistency coefficient, k (Pa·s^n)	Flow behavior index, n
Water	998	72.00	0.0010	1.0000
0.1%CMC	1000	65.62	0.0334	0.7410
0.2%CMC	1001	64.93	0.1038	0.6554
0.3%CMC	1002	63.02	0.1284	0.6618

The calculation formulas of the liquid phase dynamic Reynolds number (Re^*_L)[8], dynamic Weber number (We) and dynamic capillary number (Ca^*_L) in the microchannel are as follows:

$$Re_L^* = \frac{8^{1-n}\rho_L d v_L^{2-n}}{k}\left(\frac{n}{a+bn}\right)^n \tag{2}$$

$$We = \frac{\rho_L d v_L^2}{s} \tag{3}$$

$$Ca_L^* = \frac{We}{Re_L^*} \tag{4}$$

where ρ_L is the liquid density(kg/m^3); d is the hydraulic diameter (300 μm); v_L is the liquid velocity (m/s); a and b are constants related to the section type of the microchannel, for square section, a = 0.2121, b = 0.6766.[21]

The calculation formula of the pressure gradient (pressure drop per unit length) P_d (Pa/mm) is as follows:

$$P_d = \frac{P_D}{S} \tag{5}$$

where P_D is the pressure drop between the two pressure monitoring points (Pa), and S is the distance between the two pressure monitoring points (mm)

3.1 Pressure drop of single-phase flow

The relationship between the pressure gradient of the single-phase flow in the serpentine microchannel (P_{sd}) and the liquid flow rate (Q_L) and Weber number (We) is shown in Figure 3. With the increase of the Q_L, the P_{sd} gradually increases. The Q_L is between 0 ml/min~2 ml/min, and the CMC solution shows the phenomenon of shear-thinning (gradual decrease in the curve slope). During 2 ml/min~4 ml/min, the P_{sd} of CMC solution has the same trend as the P_{sd} of water. When the shear-thinning fluid has a high shear rate, the fluid will enter a high-shear-rate viscosity plateau [22]. When the inlet flow rate is greater than 2 ml/min, the calculated fluid shear rate ($8v_L$/d) reaches 8000~9000s^{-1} [23], consistent with the shear rate in the stable viscosity zone measured by the rheometer. Since the Weber number expression contains the quadratic of the velocity, its value is more affected by the velocity term, and the observed shear-thinning phenomenon is apparent. As shown in Figure 3(b), when We < 0.65(v_L < 0.36 m/s), the increase rate of P_{sd} gradually slows down, when We > 0.65(v_L > 0.36 m/s), the slope of the P_{sd} curve of CMC solution is basically the same as that of water.

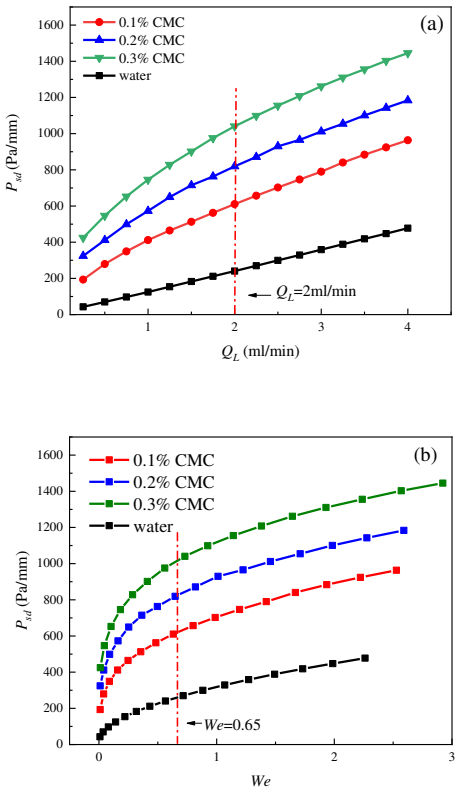

Figure 3 Relationship between P_{sd} and Q_L and We in serpentine microchannel

The relationship between the P_{sd} and the Re^*_L is shown in Figure 4(a). As the Re^*_L increases, the P_{sd} gradually increases. When Re^*_L < 17(v_L < 0.36 m/s), under the condition of low Reynolds number, the P_{sd} change rate of the CMC solution gradually decreases. When Re^*_L > 17(v_L > 0.36 m/s), the change rate of P_{sd} of the CMC solution tends to be stable, showing the characteristics of a Newtonian fluid.

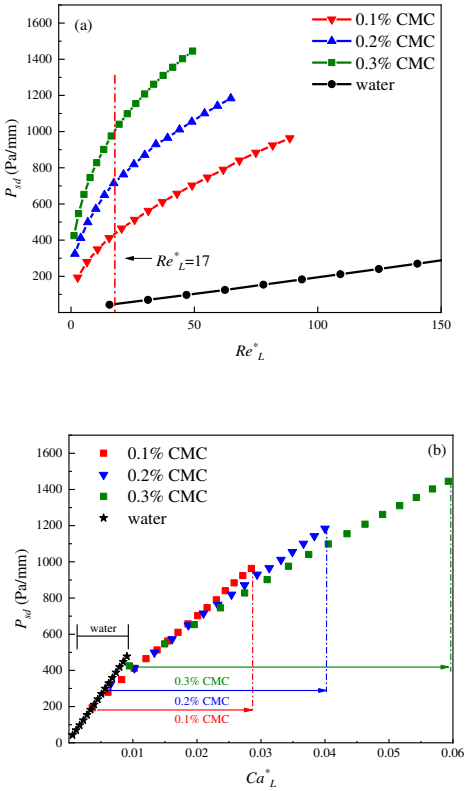

Figure 4 Relationship between P_{sd} and Re^*_L and Ca^*_L in serpentine microchannel

According to the experimental results, the P_{sd} prediction formula is fitted. The parameters of the non-Newtonian fluid characteristics and experimental conditions are added during the fitting, including viscosity and flow rate parameters[24]. The result is as follows:

$$P_{sd} = 2635 \cdot k^{0.2391} \cdot v_L^{0.0432+0.6954n} \tag{6}$$

The relationship between the P_{sd} and the Ca^*_L is shown in Figure 4(b). The P_{sd} can be partitioned by the Ca^*_L, and then the appropriate solution concentration and flow parameters can be selected according to the required pressure drop. Newtonian fluid (water) is in the left measurement area, non-Newtonian fluid is in the right area: the greater the concentration, the more comprehensive the pressure value distribution range. The Ca^*_L and the P_{sd} are closer to the relationship of the power function. The fitting formula of the experimental results is as follows:

$$P_{sd} = 9866 \cdot Ca_L^{*0.6639} \tag{7}$$

Compared with the experimental data, the mean percentage error and the root mean square percentage error of the predictions[24] for formula (6) are -1.0% and 10%, respectively. For formula (7), the errors are -6.1% and 17.2%, respectively.

For single-phase flow, using a fitting formula including viscosity and flow rate parameters is better for the prediction of P_{sd} in this experiment.

3.2 Two-phase flow pressure drop

The relationship between pressure gradient of the two-phase flow in the serpentine microchannel (P_{td}) and the Re^*_L is shown in Figure 5. For the N_2-water two-phase flow shown in Figure 5(a), the larger the Re^*_L of water, the greater the P_{td} value. The greater the gas flow rate (Q_G), the smaller the P_{td} is. When the Q_L is 2 ml/min, the Q_G is increased from 0.25 ml/min to 4 ml/min, the P_{td} decreases by 44.6%. The P_{td} of the N_2-CMC two-phase flow is shown in Figure 5(b). As the Re^*_L increases, the P_{td} gradually increases. The P_{td} of the N_2-CMC solution two-phase flow within the experimental range is almost unaffected by the Q_G. When the Q_L is 2 ml/min, and the Q_G is increased from 0.25 ml/min to 4 ml/min, the P_{td} of the three CMC solutions (0.1%, 0.2%, 0.3%) is only decrease by 4.0%, 4.1%, 5.7%. The slope of the P_{td} curve of N_2-CMC solution two-phase flow gradually decreases, when $Re^*_L > 6$($v_L > 0.16$ m/s), the slope of the curve is basically unchanged. Similar to the experimental results of the pressure drop of single-phase flow, the greater the concentration of CMC solution, the more obvious the influence of shear-thinning characteristics on the pressure drop characteristics of two-phase flow.

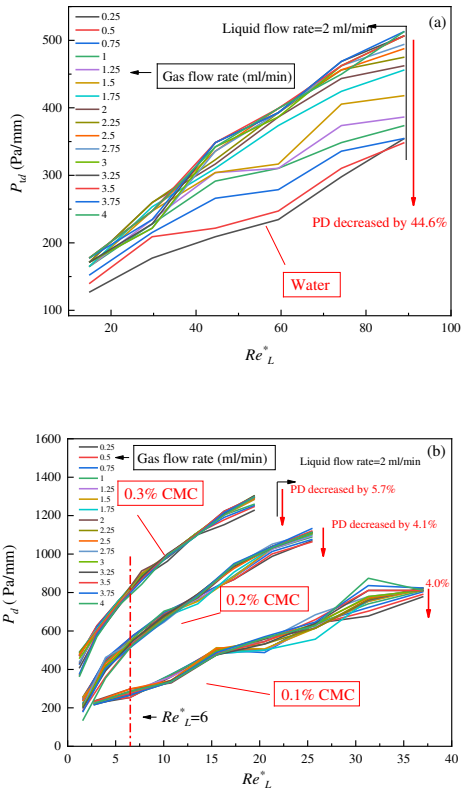

Figure 5 Relationship between P_{td} and Re^*_L in serpentine microchannel

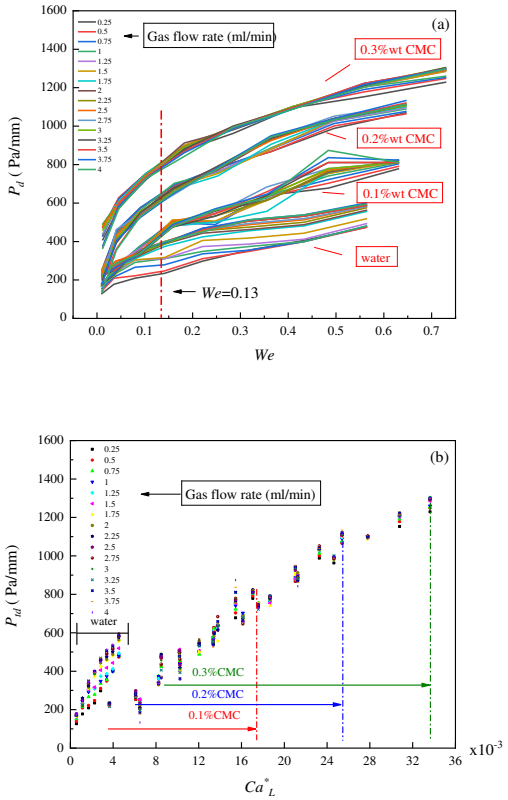

Figure 6 Relationship between P_{td} and We and Ca^*_L in serpentine microchannel

The relationship between P_{td} and We is shown in Figure 6(a). The P_{td} of the gas-liquid two-phase flow changes with the We similar to that of the single-phase flow. The mutual promotion of gas and liquid increase the overall flow velocity in the channel [25], so that when the We > 0.13(v_L > 0.16 m/s), it enters the high shear rate viscosity plateau in advance(compared with single-phase We > 0.65), showing shear-thinning characteristics. The slope of the P_{td} curve of N_2-CMC solution is basically the same as that of water when We > 0.13. The relationship between the P_{td} and the Ca^*_L is shown in Figure 6(b). The Ca^*_L can also partition the experimental results. Water is in the left measurement area, and non-Newtonian fluids are in the right area: the greater the concentration, the more comprehensive the distribution range of the P_{td}. The P_{td} range of the CMC solution with higher concentration will cover most of the CMC solution with lower concentration. P_{td} values within(0~1400 Pa/mm) can be obtained by two-phase flow when Ca^*_L < 0.035 or We < 0.8. However, P_{sd} values within (0~1400 Pa/mm) can be obtained by single-phase flow when Ca^*_L < 0.055 and We < 3.0. The experimental results show that a more extensive pressure drop range can be obtained by the gas-liquid two-phase flow when the flow rate of non-Newtonian fluid cannot be too large due to the limited flow rate in practical applications. It also shows that with the same liquid flow rate, the pressure drop of the gas-liquid two-phase flow is greater than that of the single-phase flow.

According to the experimental results, the P_{td} prediction formula of two-phase is fitted. The parameters of the non-Newtonian fluid characteristics and experimental conditions are also added during the fitting compared with formula (6). The result is as follows:

$$P_{td} = 25.87 \cdot \left(\frac{k}{\mu_G}\right)^{0.4029} \cdot \left(\frac{v_L}{v_G}\right)^{0.2058-0.0339n} \tag{8}$$

where μ_G is the gas viscosity (Pa·s), v_G is the gas velocity(m/s). The data points of N_2-water are not used in the fitting, they will cause the residual of the fitting formula to be too large.

The Ca^*_L and the P_{td} of N_2-CMC are also closer to the power function relationship. The fitting formula of the experimental results is as follows：

$$P_{td} = 13438 \cdot Ca_L^{*0.7282} \tag{9}$$

The mean percentage error and the root mean square percentage error of the formula (8) are -15.6% and 52.4%, respectively. For formula (9), the errors are -1.0% and 18.4%, respectively.

For two-phase flow, using a power function including Ca^*_L is better for the prediction of P_{td} in this experiment.

3.3 Length of bubbles generated by two-phase flow

The force involved in the bubble generation at the cross is shown in Figure 7(a).

When gas moves in the channel, in addition to its inertial force, it is also affected by the viscous force of the solution and the pressure acting on the bubblehead. When the bubble passes through the intersection, the liquid entering from the upper and lower sides exerts shear force and inertial force on the bubble and forces the neck of the bubble to become smaller.

As shown in Figure 7(b), when the width of the neck (W_d) reaches the minimum, the gas is clipped, and a bubble is formed. Gas fracture is due to the Rayleigh-Plateau instability [26]. That is, if the surface tension is neglected, the interface between two fluids of different densities

moving in parallel at different speeds will be unstable at all rates. Surface tension can offset this unstable state. Before the shear force exceeds the threshold, the system is stable (no fracture). When the generation process is pulled long enough, the shear force exceeds the threshold and bubbles are generated. During the bubble generation process, the neck continues to shrink until it breaks. Affected by the surface tension of the liquid, the bubble will be shortened to varying degrees from the break to the bubble generation.

To remove the influence on the experimental value of the bubble length, set the distance between entering the cross and the farthest position before the gas breaks as *Lt, Lt-d* is defined as the bubble length (L) after the bubble is formed [27].

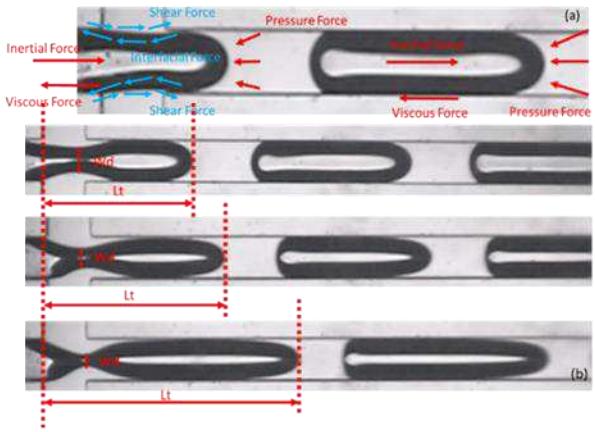

Figure 7 Bubble formation

The relationship between the length of the generated bubble(L) and the Re^*_L is shown in Figure 8(a~d). Under the same working conditions, the experimental data points are scattered in the range of $Re^*_L < 120$, due to the low water viscosity. The viscosity of the CMC solution is relatively high, so the Re^*_L is small, and the data points are densely distributed in $Re^*_L < 40$. Within the range, the higher the concentration of the solution, the denser the data points. Under the conditions of this experiment, the N_2-CMC two-phase flow can obtain the L value with higher resolution (L < 2500 μm) in the lower Reynolds number range than the N_2-water two-phase flow.

As the Q_G increases, the L increases. As the Re^*_L increases, the L of N_2-water and N_2-CMC solution gradually decreases. Consistent with the results of P_d, due to the influence of the shear-thinning characteristics of the CMC solution, the slope of the curve decreases continuously. The curve tends to be flat when $Re^*_L > 6$ ($v_L > 0.16$ m/s).

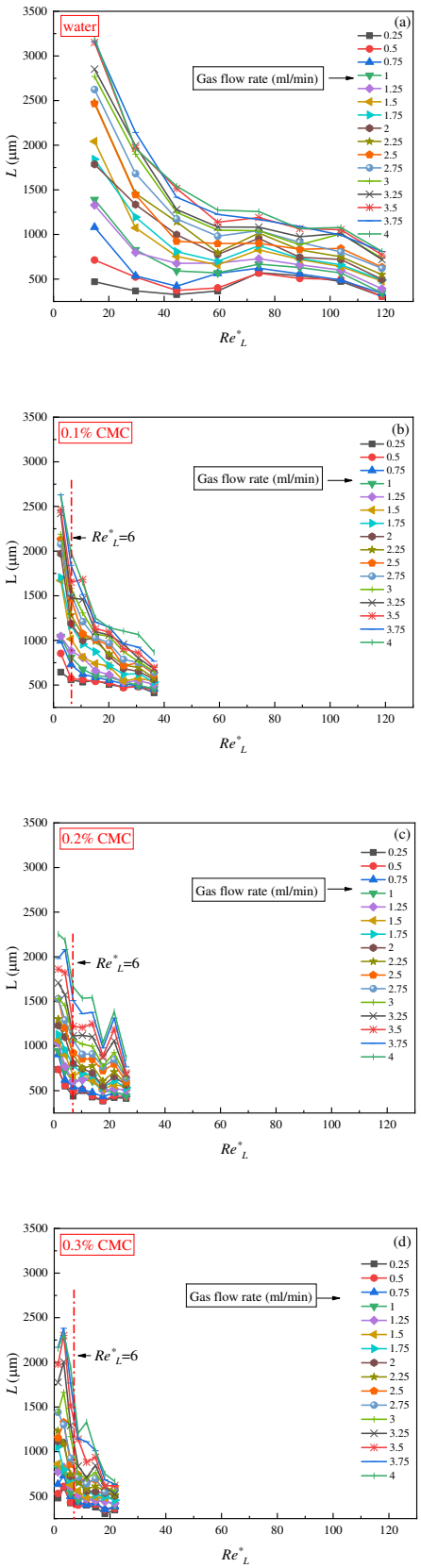

Figure 8 The relationship between L and the Re^*_L

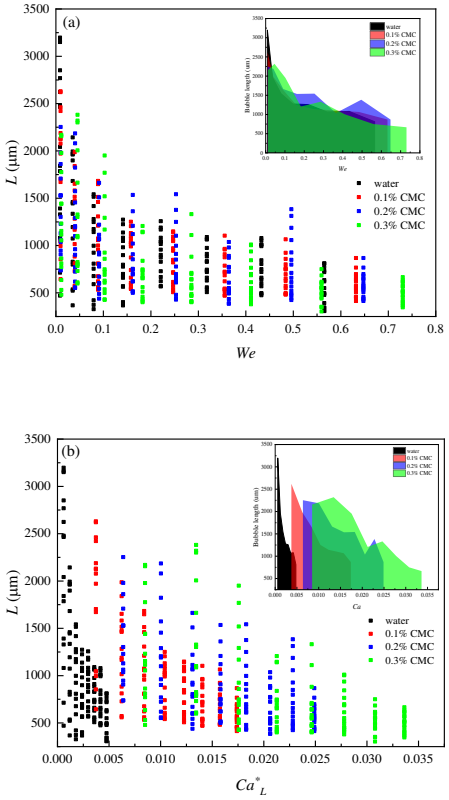

Figure.9 Relationship between L at intersections and the We and Ca^*_L

The relationship between the L and the We is shown in Figure 9(a). The numerical distribution of the N_2-water two-phase flow is similar to the N_2-CMC solution two-phase flow. With the increase of We, the L gradually decreases, the bubble length of N_2-water and N_2-CMC two-phase flow basically coincides, so the generated bubble length can be controlled uniformly by controlling the Weber number of the non-Newtonian fluid and the Newtonian fluid.

The relationship between L and Ca^*_L is shown in Figure 9(b). Similar to the conclusion of single-phase flow and two-phase flow pressure drop, the data can be partitioned in the x-axis direction. The greater the CMC solution concentration, the greater the coverage is. If the required bubble length is constant, a high-concentration CMC solution can have a more extensive value range of Ca^*_L than water and low-concentration CMC solutions.

3.4 The relationship between pressure drop and bubble length

It is found that the length of the bubble will increase when it moves in the channel after the bubble is generated. During the bubble generation process, internal gas is squeezed by the outside to compress the volume of the bubble. As the distance of bubble movement increases, the pressure of the environment where the bubble is located is reduced. The pressure on the bubblehead is reduced to stretch the compressed gas, and the bubble volume increases.

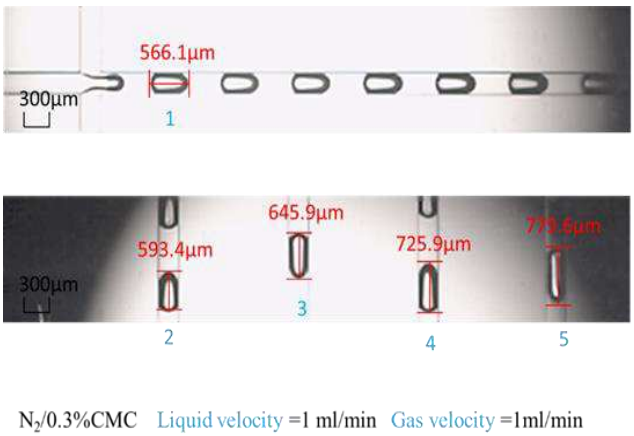

Figure 10 The change in the length of a bubble as it moves through the channel

As shown in Figure 10, taking the experimental conditions as N_2-0.3% CMC, the Q_L and Q_G are both 1ml/min as an example. The L at position 1 is 566.1 μm after the bubble is formed. The L at positions 2, 3, 4, and 5 are 593.4 μm, 645.9 μm, 725.9 μm, and 779.6 μm, respectively.

The CFD method was used to simulate the bubble generation and transfer process in the microchannel. The results are shown in Figure 11. It can be seen from the phase diagram that the bubble length increases because of the pressure drop.

By observing the velocity pathlines, it shows that two small vortices are formed on both sides of the bubblehead after generation. The velocity value is greater than the other parts of the bubble. When it reaches position 2, the bubble has undergone a turn. The two vortices at the head of the bubble merge into a larger vortex and deviate to the turning side. When it reaches position 5, the size and speed of the vortex at the head of the bubble increase slightly. By observing the velocity vector diagram, it shows that the velocity of the bubblehead moving from position 1 to position 5 gradually increases and the tail tends to extend to the back of the bubble. By observing the static pressure graph, it shows that the pressure on both sides of the bubble gradually decreases with the movement, which is beneficial to expanding the bubblehead and tail.

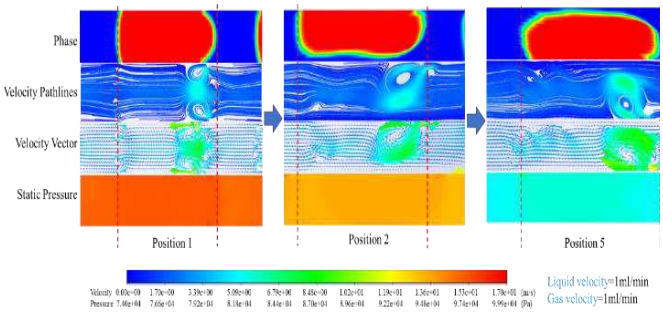

Figure 11 Numerical simulation of bubble length change

L1 is a line passing through the channels at positions 2, 3, 4, and 5 in Figure 1. A high-speed camera was used to capture the change of L when a bubble moves from 2 to 5($\triangle L$), and calculate the pressure drop between 2 and 5(P_D*). The numerical calculation formula is as follows:

$$P_D^* = \frac{P_D S^*}{S} \tag{10}$$

where S* is the distance of bubble movement from position 2 to 5.

The relationship between $\triangle L$ and P_d* of water and three CMC solutions is shown in Figure 12. $\triangle L$ is all positive, indicating that the volume of the bubble will increase after passing a certain distance under any conditions. For non-Newtonian fluids, the $\triangle L$ of the two-phase flow of the three CMC solutions decreases with the increase in P_d*. The smaller concentration of CMC solution, the more obvious the phenomenon. The $\triangle L$ of N_2-water two-phase flow is not significantly affected by the pressure drop. When Q_L = 1 ml/min of the four gas-liquid two-phase flows, as shown in data points in the box in Figure 12, the larger the v_G, the larger the $\triangle L$. The initial volume of the bubble generated has a significant influence on the value of $\triangle L$, and the same conclusions can be made for other Q_L.

According to the common sense, the larger the pressure drop, the more significant $\triangle L$ should be. However, it is found in the experimental results that the larger the pressure drop, the more concentrated the data points of $\triangle L$ are in the smaller numerical range. The reason is that while the pressure drop in the channel is large, the liquid velocity is also significant. The resistance to the gas expansion in the bubble is greater, and it is more difficult for the bubbles to increase their volumes. It can only be said that the pressure drop is the inducement for the change of bubble length. The inlet gas velocity is the main influencing factor of the value of $\triangle L$.

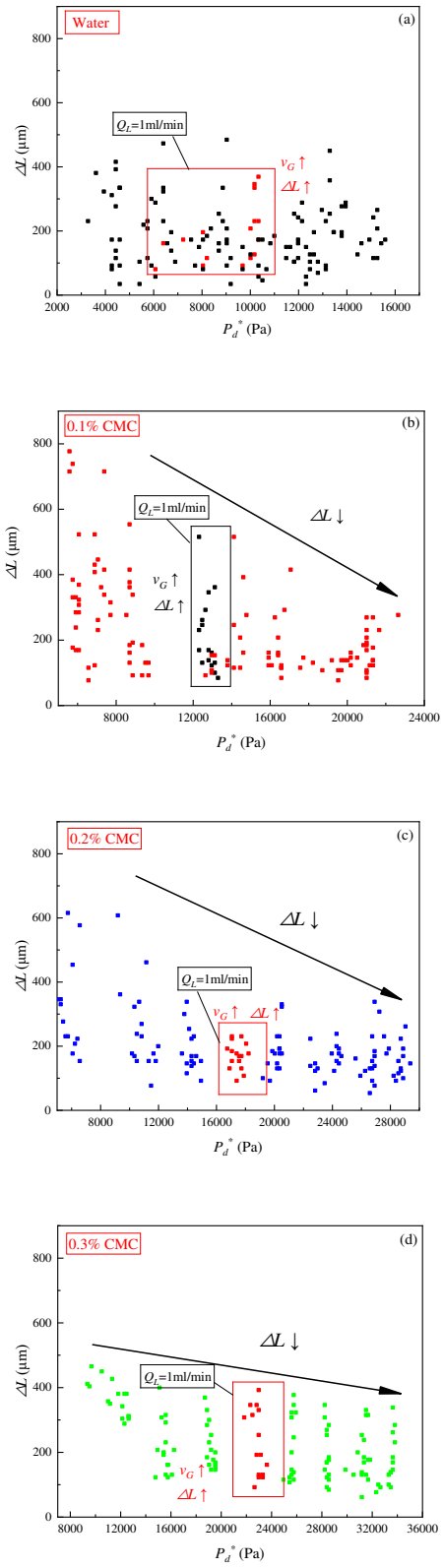

Figure 12 Relationship between $\triangle L$ and P_d*

4 Conclusions

(1) The fitting formulas for the pressure drop gradient of the single-phase are given. Pressure drop gradient of single-phase flow increases with the Re^*_L and We. The single-phase flow of CMC solution shows characteristics of shear-thinning when Re^*_L >17 and We > 0.65. At this time, the change rate of pressure drop gradient is the same as that of water. Ca^*_L can be used to divide the pressure drop gradient of non-Newtonian fluid and the Newtonian fluid single-phase flow into regions to obtain the required pressure drop value.

(2) The fitting formulas for the pressure drop gradient of the two-phase are given. Pressure drop gradient of the two-phase flow increases with the Re^*_L and We. The higher the gas velocity in the N_2-water two-phase flow, the smaller the pressure drop gradient. The pressure drop gradient of the N_2-CMC two-phase flow changes to the gas velocity insensitively. The N_2-CMC solution two-phase flow shows shear-thinning characteristics when Re^*_L > 6 and We > 0.13. Ca^*_L can be used to divide the pressure drop gradient of non-Newtonian fluid and Newtonian fluid two-phase flow into regions. With the same liquid flow rate, the pressure drop gradient of the two-phase flow is greater than that of the single-phase flow.

(3) With the increase of Re^*_L and We, the bubble length decreases gradually. A higher resolution of the bubble length value can be obtained at lower Re^*_L by using the N_2-CMC two-phase flow. Ca^*_L can be used to divide the bubble length of non-Newtonian and Newtonian fluid into regions. We can be used to obtain both non-Newtonian and Newtonian bubble length. When the bubble moves in the channel, it is lengthened by the pressure drop. The pressure drop is the inducement of the change in the length of the bubble. The inlet gas velocity has a significant effect on the change of bubble length.

5 Declaration

Funding

Supported by National Natural Science Foundation of China (Grant No. 51775077)

Availability of data and materials

The datasets supporting the conclusions of this article are included within the article.

Authors' contributions

The author' contributions are as follows: Hui-Chen Zhang and Gang Yang were in charge of the whole trial; Gang Yang wrote the manuscript; Kai Feng, Jia-Pei Li, Yu-Hang Gao assisted with sampling and laboratory analyses.

Competing interests

The authors declare no competing financial interests.

Consent for publication

Not applicable

Ethics approval and consent to participate

Not applicable

References

[1]. Nguyen N T. Micromixers: Fundamentals, Design, and Fabrication. William Andrew Pub, 2011.

[2]. Huang J, Zhang J, Shi W, Wang Y. 3D FEM analyses on flow field characteristics of the valveless piezoelectric pump. Chinese Journal of Mechanical Engineering. 2016;29(4): 825-831.

[3]. Huang J, Zhang J, Wang S, Liu W. Analysis of the flow rate characteristics of valveless piezoelectric pump with fractal-like Y-shape branching tubes. Chinese Journal of Mechanical Engineering. 2014, 27(3): 628-634.

[4]. M Poux, P Cognet, C Gourdon Green Process Engineering: From Concepts to Industrial Applications, CRC press, 2015.

[5]. Tao Y, Ren Y, Yan H, Jiang H. Continuous separation of multiple size microparticles using alternating current dielectrophoresis in microfluidic device with acupuncture needle electrodes. Chinese Journal of Mechanical Engineering. 2015, 29(2): 325-331.

[6]. Guo L, Zhang S, Cheng L. Study on characteristics of vapor–liquid two-phase flow in mini-channels. Nuclear Engineering and Design 2011, 241(10): 4158-4164.

[7]. W M Wang, Y P Ma, B Chen. Numerical simulation of droplet formation in cross microchannel. CIESC Journal, 2015, 66(5): 1633-1641. (in Chinese)

[8]. Mansour M H, Kawahara A, Sadatomi M Experimental investigation of gas–non-Newtonian liquid two-phase flows from T-junction mixer in rectangular microchannel. International Journal of Multiphase Flow 2015, 72: 263-274.

[9]. Laporte M, Montillet A, Belkadi A, Della Valle D, Loisel C, Riaublanc A, Hauser J L. Investigation of gas/shear-thinning liquids flow at high throughput in microchannels with the aim of producing biosourced foam. Chemical Engineering and Processing - Process Intensification 2020, 148: 107787.

[10]. Guo R, Fu T, Zhu C, Ma Y. Pressure drop model of gas-liquid flow with mass transfer in tree-typed microchannels. Chemical Engineering Journal 2020, 397: 125340.

[11]. Mondal S, Majumder S K Frictional pressure drop of aqueous-organic two-phase flow through packed and unpacked rectangular serpentine millichannel. Experimental Thermal and Fluid Science 2018, 94: 215-230.

[12]. Lewis J M, Wang Y. Two-phase frictional pressure drop and water film thickness in a thin hydrophilic microchannel. International

Journal of Heat and Mass Transfer 2018, 127: 813-828.
[13]. Li X, Hibiki T. Frictional pressure drop correlation for two-phase flows in mini and micro multi-channels. Applied Thermal Engineering 2017, 116: 316-328.
[14]. Santoso A, Goto D, Takehira T., Aslam A., Kawahara A., Sadatomi M. Non-Newtonian Two-Phase Flow Characteristics across Sudden Expansion in Horizontal Rectangular Minichannel. World Journal of Mechanics 2016, 06(8): 257-272.
[15]. Han W, Chen X. New insights into the pressure during the merged droplet formation in the squeezing time. Chem. Eng. Res. Des. 2019.145: 213–225.
[16]. Han W, Chen X, Wu Z, Zheng Y. Three-dimensional numerical simulation of droplet formation in a microfluidic flow-focusing device. Journal of the Brazilian Society of Mechanical Sciences and Engineering 2019, 41(6): 265-275.
[17]. Zhou H, Zhu C, Fu T, Ma Y, Li HZ. Dynamics and interfacial evolution for bubble breakup in shear-thinning non-Newtonian fluid in microfluidic T-junction. Chemical Engineering Science. 2019, 208: 115158.
[18]. Rostami B, Morini G L. Experimental characterization of a micro cross-junction as generator of Newtonian and non-Newtonian droplets in silicone oil flow at low Capillary numbers. Experimental Thermal and Fluid Science 2019, 103: 191-200.
[19]. Zhen Cao, Zan Wu, Bengt Sundén Dimensionless analysis on liquid-liquid flow patterns and scaling law on slug hydrodynamics in cross-junction microchannels, Chemical Engineering Journal 2018, 344: 604–615.
[20]. Somasekhara G S, Arnab A. CFD analysis of microfluidic droplet formation in non–Newtonian liquid, Chemical Engineering Journal 2017, 330: 245–261.
[21]. Shah, R.K., London, A.L. Chapter VII - rectangular ducts. In: Laminar Flow Forced Convection in Ducts. Academic Press, 1978
[22]. Ansari S, Rashid M A I, Waghmare P R, Nobes D S. Measurement of the flow behavior index of Newtonian and shear-thinning fluids via analysis of the flow velocity characteristics in a mini-channel. SN Applied Sciences 2020, 2(11):1787.
[23]. Younggong S. Determination of shear viscosity and shear rate from pressure drop and flow rate relationship in a rectangular channel. Polymer 2007, 48: 632-637.
[24]. Feng K, Zhang H. Pressure drop and flow pattern of gas-non-Newtonian fluid two-phase flow in a square microchannel. Chemical Engineering Research and Design. 2021, 173:158-169.
[25]. Faghri A, Zhang Y. Fundamentals of Multiphase Heat Transfer and Flow. Publisher: Springer International Publishing, Switzerland, 2020: 551-554.
[26]. Wu P, Luo Z, Liu Z, Li Z, Chen C, Feng L, He L. Drag-induced breakup mechanism for droplet generation in dripping within flow focusing microfluidics. Chinese Journal of Chemical Engineering 2015, 23 (1): 7-14.
[27]. Costa A L R., Gomes A, Cunha R L. Studies of droplets formation regime and actual flow rate of liquid-liquid flows in flow-focusing microfluidic devices. Experimental Thermal and Fluid Science 2017, 85: 167-175.

Biographical notes

Gang Yang, born in 1996, is currently a Ph.D. candidate at *Naval Architecture and Ocean Engineering College, Dalian Maritime University, China.* He received his bachelor's degree from *Fuzhou University, China*, in 2018. His research interests focus on microfluidic devices.
Tel: +86-18641125619; E-mail: 1186593481@qq.com

Kai Feng, born in 1988, is currently a Ph.D. candidate at *Naval Architecture and Ocean Engineering College, Dalian Maritime University, China.*
E-mail: fengkai@dlmu.edu.cn

Jia-Pei Li, born in 1994, is currently a master candidate at *Naval Architecture and Ocean Engineering College, Dalian Maritime University, China.*
E-mail: 504961331@qq.com

Yu-Hang Gao, born in 1996, is currently a master candidate at *Naval Architecture and Ocean Engineering College, Dalian Maritime University, China.*
E-mail: 3222511387@qq.com

Hui-Chen Zhang, born in 1965, is currently a professor and a Ph.D. candidate supervisor at *Naval Architecture and Ocean Engineering College, Dalian Maritime University, China.* He received his bachelor's degree and master's degree from *Shenyang Polytechnic University, China*, in 1987 and 1990, respectively. He received his Ph.D. degree in mechanical design and theory from *Xi'an Jiaotong University, China*, in 1993. His research interests focus on microfluidic devices and nanotribology.
Tel: +86-15542672593; E-mail: hczhang@dlmu.edu.cn

Appendix

Appendix and supplement both mean material added at the end of a book. An appendix gives useful additional information, but even without it the rest of the book is complete: In the appendix are forty detailed charts. A supplement, bound in the book or published separately, is given for comparison, as an enhancement, to provide corrections, to present later information, and the like: A yearly supplement is issue.